

## First Observation of the Neutron-Rich Isotope $^{19}\text{B}$

J. A. Musser<sup>(a)</sup> and J. D. Stevenson<sup>(b)</sup>

*Department of Physics, University of California, Berkeley, California 94720*

(Received 2 August 1984)

The particle stability of  $^{19}\text{B}$  and the particle instability of  $^{18}\text{B}$  are demonstrated. Light neutron-rich nuclei were searched for among the projectile fragments resulting from interactions of a 670-A-MeV  $^{56}\text{Fe}$  beam in a 7.9-g/cm<sup>2</sup> Be target. A detector consisting of a magnetic spectrometer, threshold Cherenkov paddles, and scintillator paddles was used to determine the charge and mass of the projectile fragments.

PACS numbers: 27.20.+n, 23.90.+w, 25.70.Np

Establishing the limits of particle stability for nuclei has been a goal of experimenters for many years. As a result of their work, it is believed that all particle-stable isotopes with charge  $Z < 5$  have been observed. The most neutron-rich boron isotope previously observed to be particle stable is  $^{17}\text{B}$ .<sup>1</sup> In the same experiment  $^{16}\text{B}$  was shown to be unstable to prompt neutron emission. Current nuclear-mass models<sup>2-5</sup> which can be applied to very light nuclei indicate that this even-odd gap structure should continue through  $^{18}\text{B}$  and  $^{19}\text{B}$ , and that  $^{19}\text{B}$  should be the most neutron-rich particle-stable boron isotope. Our result is the first experimental confirmation of the particle stability of  $^{19}\text{B}$  and particle instability of  $^{18}\text{B}$ .

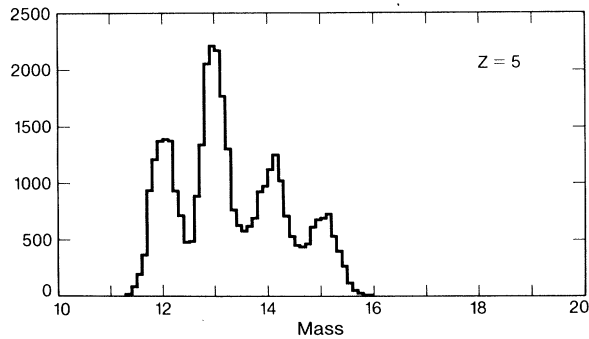
In recent years a powerful technique has been developed for producing rare isotopes, using projectile fragmentation of relativistic heavy ions.<sup>6,7</sup> Projectile fragmentation occurs in large-impact-parameter collisions of a high-energy heavy ion with a stationary target nucleus. The distinguishing characteristic of this type of interaction is the presence of a high- $Z$  remnant of the projectile in the projectile frame. These fragments can possess any combination of charge and mass compatible with the number of neutrons and protons in the projectile.

The properties of projectile fragmentation have been extensively studied, primarily at Lawrence Berkeley Laboratory's Bevalac. The salient characteristics of projectile fragmentation from the standpoint of rare-isotope production are the projectile fragment's transverse- and longitudinal-momentum distributions and isotopic-production cross sections. Projectile fragments viewed in the projectile frame have Gaussian transverse- and longitudinal-momentum distributions with widths  $\sigma_{\parallel} \approx \sigma_{\perp} \approx 200 \text{ MeV}/c$ .<sup>8</sup> In the laboratory frame the fragments are confined to  $\sim 1^\circ$  about the beam direction, and have velocities within a few percent of that of the projectile. The "beamlike" behavior of projectile fragments represents the primary advan-

tage of projectile fragmentation over previous methods used to produce rare isotopes, such as spallation reactions in high-energy proton-nucleus collisions. The isotopic distribution of projectile fragments of a given charge is roughly Gaussian, with the most abundant isotope having a mass between  $A_{\text{frag}} = 2Z_{\text{frag}}$  and  $A_{\text{frag}} = (A/Z)_{\text{proj}}$ . The isotopic distribution typically has a width  $\sigma_A \approx 2$  amu, with the yields of very neutron-rich isotopes observed to decrease by about 1 order of magnitude per isotope for increasing mass.<sup>9</sup>

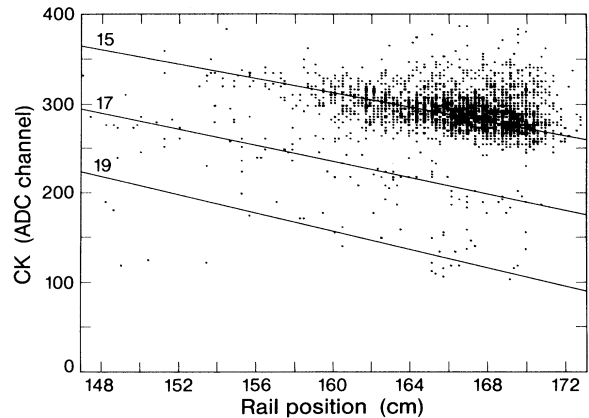
For the experiment described in this Letter, projectile fragments were produced by interactions of a 670-A-MeV  $^{56}\text{Fe}$  beam in a 7.9-g/cm<sup>2</sup> Be target. The charges and masses of the projectile fragments were obtained with use of the  $0^\circ$  spectrometer facility at the Bevalac in conjunction with a detector telescope (described in detail elsewhere<sup>10</sup>) located in the focal plane of the spectrometer. The telescope consisted of a wire-chamber hodoscope, a front scintillator paddle, a set of threshold Cherenkov counters, and a back scintillator paddle. The charges of the projectile fragments were determined by the scintillator and Cherenkov signals. Once a fragment's charge was obtained, its mass could be found from the particle's rigidity, provided by the spectrometer, in combination with the Cherenkov measurements. The back scintillator was used to reject events in which the fragment interacted in the telescope. The charge resolution of the detector was typically  $\sigma_Z = 0.1e$  and the mass resolution  $\sigma_A = 0.25$  amu.

Data were taken in a 72-h period during which a total beam fluence of  $\sim 1 \times 10^{11}$  particles was obtained. The finite rigidity acceptance of the telescope required that the detector be moved during the course of the run in order to cover a reasonably large range of charge-to-mass ratios. As a consequence of the finite telescope acceptance, the observed relative abundance of isotopes is unrelated to the relative production cross sections. Figure 1 contains a mass histogram of the boron isotopes  $^{12}\text{B}$  to  $^{15}\text{B}$  representing data taken at three rigidity inter-

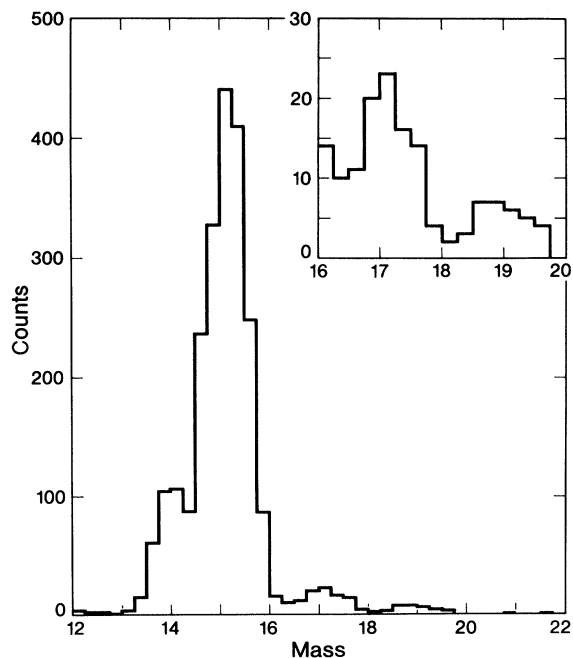
FIG. 1. Boron isotopes  $^{12}\text{B}$  to  $^{15}\text{B}$ .

vals. Although we have not measured the absolute production cross sections for these isotopes, it is likely that they decrease by 3–4 orders of magnitude in this mass interval.

The proper assignment of isotopic mass based on a set of rigidity and Cherenkov-intensity measurements was certainly the most important aspect of data analysis. This was done primarily through a very careful calibration of detector response. The response of the detector elements to a set of degraded  $^{20}\text{Ne}$  beams of precisely known energies in the range 300A to 670A MeV provided the basis for this calibration. The energies of the degraded  $^{20}\text{Ne}$  beams were determined by ranging the primary  $^{20}\text{Ne}$  beam out in a stack of 0.003-in.-thick Lexan sheets. The range of the beam was found by etching the stack in sodium hydroxide and observing the point in the stack at which the radiation damage decreased sharply, corresponding to the end of range of the beam. By use of standard range-energy relations, the beam energy was then calculated, with an uncertainty of  $\sim \pm 2A$  MeV. The measured response curves for the scintillator and Cherenkov paddles were used to fix parameters in response models developed for these detector elements. The scintillator model included the effects of response saturation associated with highly ionizing particles through the incorporation of the Birks-Tarlé-Voltz formalism.<sup>11</sup> The Cherenkov response model contained contributions to the total light output from the Cherenkov radiation of high-energy knock-on electrons produced in the radiator, and residual scintillation, as well as the primary Cherenkov radiation of the heavy ion. These models were found to provide good fits to the measured response curves of the detector elements in the energy interval of interest ( $350A < E < 650A$  MeV). In this energy range the calculated detector response agreed with the measured values to better than 1%. A typical response difference in the Cherenkov detectors for adjacent isotopes with

FIG. 2. Scatter plot of boron data in Cherenkov-rigidity plane. Also shown are the expected locations of  $^{15}\text{B}$ ,  $^{17}\text{B}$ , and  $^{19}\text{B}$ .

equal charge and velocity was  $\sim 10\%$ , implying that the systematic error in the mass assignments due to inaccuracy of the response models was  $< 0.1$  amu. With use of the detector-response models, the positions of isotopic bands in the Cherenkov-rigidity plane were correctly predicted to within  $\sim 0.1$  amu for isotopes of all charges in all data sets. The mean systematic error in the mass assignments was consistent with the precision with which the detector

FIG. 3. Histogram of boron isotopes  $^{15}\text{B}$  to  $^{19}\text{B}$ , representing data from Fig. 2. Inset:  $^{17}\text{B}$  and  $^{19}\text{B}$  counts on expanded scale.

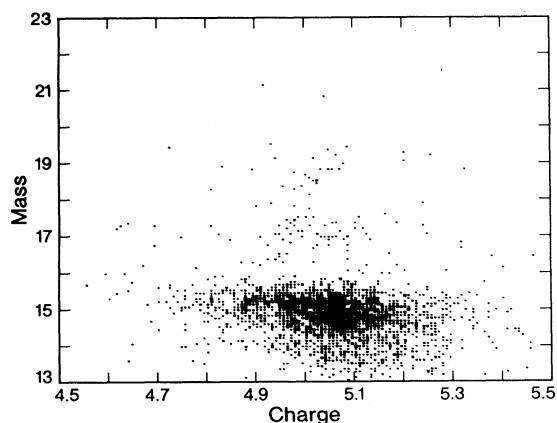


FIG. 4. Scatter plot of boron data in charge-mass plane.

telescope's position could be measured. Additional support for the validity of mass assignments based on the response models is provided by the observed particle instability of  $^{16}\text{B}$ , which is in agreement with previous observations.<sup>1</sup>

Figure 2 shows a scatter plot (in the Cherenkov-rigidity plane) of boron data taken at a single rigidity interval containing the most neutron-rich isotopes acquired. Also shown in this figure are the predicted locations of  $^{15}\text{B}$ ,  $^{17}\text{B}$ , and  $^{19}\text{B}$ . The previously observed particle instability of  $^{16}\text{B}$  and particle stability of  $^{17}\text{B}$  is apparent in this figure. In addition, our data indicate for the first time that  $^{19}\text{B}$  is particle stable, while  $^{18}\text{B}$  is unstable to prompt neutron emission. The use of a single rigidity interval guarantees that the observed gaps are real, and not an artifact associated with combining data sets. A mass histogram representing the data from Fig. 2 is displayed in Fig. 3.

The most potentially dangerous form of background to be addressed is contamination from neighboring charges. Figure 4 shows the data from Fig. 2 plotted in the charge-mass plane. It is clear from this figure that the boron data are cleanly separated from adjacent charges, and that the  $^{19}\text{B}$  events differ in no way in their charge assignments from the rest of the boron data.

The mass models developed in Refs. 2–5 predict single-particle binding energies for  $^{19}\text{B}$  in the range  $1.73 < E_b < 2.93$  MeV. The isotope  $^{18}\text{B}$  is predicted to be unbound in all models by energies in the range  $-1.62 < E_b < -1.22$  MeV. Three of the mass formulas (Refs. 2–4) are based upon various formulations of the Garvey-Kelson relations,<sup>12</sup> while the mass model of Ref. 5 is a development of the droplet model, first formulated by Meyers and

Swiatecki.<sup>13</sup> Although the quantitative agreement of these models is quite good for the boron isotopes, their particle-stability predictions begin to diverge for higher charges. It is, therefore, of interest to continue the search for new isotopes having charges  $Z > 5$ .

In conclusion, we have presented the first evidence for the particle stability of  $^{19}\text{B}$  and the particle instability of  $^{18}\text{B}$  in agreement with current mass relations. Judging from the results of this experiment, it appears possible to extend the known limits of particle stability of light neutron-rich nuclei to the predicted position of the neutron-drip line, with use of a detector such as that described here and with currently available intensities of relativistic heavy ion beams.

The authors wish to thank Steve Barwick and Mark Tincknell for valuable help during the run, and Fred Lothrop and the Bevalac staff for their outstanding efforts in the development of an intense  $^{56}\text{Fe}$  beam.

<sup>(a)</sup> Also at Lawrence Berkeley Laboratory, University of California, Berkeley, Cal. 94730.

<sup>(b)</sup> Also at Space Science Laboratory, University of California, Berkeley, Cal. 94720.

<sup>1</sup>J. D. Bowman, A. M. Poskanzer, R. G. Korteling, and G. W. Butler, *Phys. Rev. C* **9**, 836 (1974).

<sup>2</sup>C. Thibault and R. Klapisch, *Phys. Rev. C* **9**, 793 (1974).

<sup>3</sup>J. Janecke, *At. Data Nucl. Data Tables* **17**, 455 (1976).

<sup>4</sup>E. Comay and I. Kelson, *At. Data Nucl. Data Tables* **17**, 463 (1976).

<sup>5</sup>H. Groote, E. R. Mitt, and K. Takahashi, *At. Data Nucl. Data Tables* **17**, 418 (1976).

<sup>6</sup>G. D. Westfall, T. J. M. Symons, D. E. Greiner, H. H. Heckman, P. J. Lindstrom, J. Mahoney, A. C. Shotter, and D. K. Scott, *Phys. Rev. Lett.* **43**, 1859 (1979).

<sup>7</sup>J. D. Stevenson and P. B. Price, *Phys. Rev. C* **24**, 2102 (1981).

<sup>8</sup>D. E. Greiner, P. J. Lindstrom, H. H. Heckman, B. Cork, and F. S. Beiser, *Phys. Rev. Lett.* **35**, 152 (1975).

<sup>9</sup>Y. P. Viyogi, T. J. M. Symons, D. E. Greiner, H. H. Heckman, D. L. Hendrie, P. J. Lindstrom, J. Mahoney, D. K. Scott, K. van Bibber, G. D. Westfall, H. Wieman, H. J. Crawford, C. McParland, and C. K. Gelbke, *Phys. Rev. Lett.* **42**, 33 (1979).

<sup>10</sup>J. D. Stevenson and J. A. Musser, *Nucl. Instrum. Methods* **213**, 285 (1983).

<sup>11</sup>M. H. Salamon and S. P. Ahlen, *Nucl. Instrum. Methods* **195**, 557 (1982).

<sup>12</sup>G. T. Garvey and I. Kelson, *Phys. Rev. Lett.* **16**, 197 (1966).

<sup>13</sup>W. D. Meyers and W. J. Swiatecki, *Ann. Phys. (N.Y.)* **84**, 186 (1974).